Model with dynamic faulting and surface processes

The model used for the simulations reported in Figures 1-3 of the main text is based on two dimensional (plane strain) mass conservation and quasi-static force balance (including gravity) of a slowly creeping fluid that is weakly compressible (Simpson, 2006). The governing equations were solved using the Galerkin Finite Element Method on rectangles with 9 node shape functions for velocities and 4 node linear shape functions for rock pressure. The rheology was linear viscoelastic (Maxwell) or plastic (Mohr Coulomb) in different parts of the model depending on local stresses and strain rates. Deformation within the model was driven by applying boundary convergence at a rate of 2 mm/yr. Otherwise boundary-parallel free-slip boundary conditions were applied at the base and sides of the model while the top surface is free to deform. All calculations were performed with the following parameters: Young's modulus, $E=10^{10}$ Pa, Poisson's ratio, $\nu=0.3$, viscosity and density of lower layer, $\mu=10^{21}$ Pa s, $\rho=3300$ kg/m^3, viscosity and density of upper layer, $\mu=10^{32}$ Pa s (implying that this layer behaves as an elastic-plastic material), $\rho=2800$ kg/m^3, angle of internal friction $\phi=30°$, cohesion $c= 25\text{x}10^6$ Pa, sediment density $\rho=2500$ kg/m^3. These parameters are relatively well constrained on the basis of rock deformation experiments (e.g., see Jaeger et al., 2007).

Surface changes caused by erosion and sedimentation were treated by solving:

$$\frac{Dh}{Dt} = \frac{\partial}{\partial x}\left[\left(\kappa + c{q_w}^n\right)\frac{\partial h}{\partial x}\right] \qquad (1)$$

where h is the surface elevation, t is the time, κ ($=10^{-7}$ m^2/s) is the linear hillslope diffusivity, c ($=8$ (m^2/s)$^{1-n}$) is a fluvial erosion coefficient, n ($=2$) is an exponent that describes the dependency of sediment discharge on fluid transport and q_w is the water discharge per unit width. D/Dt represents the substantive time derivative computed in the reference frame of the deforming substrate. The water discharge was calculated by integrating the following mass balance relation for surface water away from local drainage divides:

$$\frac{\partial q_w}{\partial x} = \alpha \qquad (2)$$

where α is the mean rainfall rate in excess of infiltration. This study illustrates simulations performed with two different rainfall rates: α = 0.274 mm/hr which drives efficient surface processes, and α = 0.0685 mm/hr (a factor of 4 less), for which surface processes are relatively inefficient. Equations 1 and 2 provide a simple means of coupling climate (rainfall) with local and long range sediment transport (Simpson and Schlunegger, 2003).

Two different model setups were investigated (Fig. DR1 A & B). Both setups considered a 600 km wide by 60 km deep domain consisting of a 30 km thick crust (ρ=2800

kg/m^3) resting on a more dense mantle (ρ =3300 kg/m^3). In the first case, the mantle behaves as a weak Maxwell viscoelastic fluid (viscosity = 10^{21} Pa s) while the entire crust is elastoplastic (Mohr-Coulomb) and thus deforms by elastic flexing and/or plastic strain localization (Fig. DR1A). In the second case, the lower 10 km of the crust also behaves viscoelastically, while only the upper 20 km of the crust is elastoplastic. The results of the two setups are similar, except that the widths of the basins and mountains are narrower when the thickness of the brittle layer is decreased (e.g. compare Fig. 1 in main text with Fig. DR6).

Flexural modeling

Flexural profiles (presented in Figures 1 and DR6) were computed by numerically solving the flexure equation:

$$D\frac{\partial^4 w(x)}{\partial x^4} + \Delta\rho g w(x) = q(x) \qquad (3)$$

where *w(x)* is the vertical deflection, *x* is the horizontal distance, *q(x)* is load due to topography, $\Delta\rho$ is the density difference between the rocks below and above the elastic plate (i.e., 3300-2500=800 kg/m^3), *g* is the acceleration due to gravity and *D* is the flexural rigidity defined as:

$$D = \frac{E\,T^3}{12(1-\nu^2)}$$

where *E* is Young's modulus (10^{10} Pa), ν is Poisson's ratio (0.3) and *T* is the thickness of the upper elastic-plastic layer (30 km in Fig. 1, 20 km in Figs. DR3-DR5). The plate was assumed to be fixed at the left boundary located far from loads, while it was considered to terminate (i.e., it is broken) where the base of the upper crust in the overthrust block intersects the top of the lower block. The spatially variable topographic load was computed as the weight of all rocks residing above the elevation of the foreland basin. Note that in the flexural calculation, the sediment load is not explicitly included in the topographic load. Rather it is assumed that the flexural depression fills entirely with sediment of density 2500 kg/m^3, which is treated by appropriate choice of $\Delta\rho$ in equation (3) above.

Viscoelastic kinematic fault model

A semi-kinematic fault model with a viscoelastic rheology was used in this study to better understand controls on fault-induced deformation. The finite element model considers an elastic plate (lithosphere) resting on a viscoelastic material. A discrete planar fault with a certain dip and slip magnitude is prescribed to cut the upper elastic layer. The displacement discontinuity simulating a fault is implemented with the split node technique (Melosh and Raefsky, 1981). This type of model can be considered to account for coseismic deformation and postseismic relaxation, but it neglects interseismic deformation related to far-field tectonic convergence, as considered in the more complete dynamic fault model described

above. Also, in these models, I consider only one discrete slip event, not the complete time evolution of the mountain-basin system. Thus, while the slip magnitude controls subsidence in the one-step kinematic model, in the time-evolving dynamic fault model the slip rate determines the subsidence rate in the foreland basin.

Calculations were performed with a model domain 600 km wide by 300 km deep and the following parameter values: upper elastic plate (ρ =2800 kg/m^3, E=10^{10} Pa, ν=0.49), lower viscoelastic material (ρ =3300 kg/m^3, μ =10^{20} Pa s, E=10^{10} Pa, ν=0.49). These parameters imply that the Maxwell relaxation time ($\tau=2(1+\nu)\mu/E$) of the viscoelastic medium is about 1000 years. Relaxed solutions are presented after 30τ, or about 30,000 years. Because I focus on fully relaxed solutions, these calculations can be considered equivalent to those for a purely elastic layer resting on an inviscid substrate (i.e., there are no viscous, time dependent, effects).

Results computed with this model presented in Figure DR7 show that faulting induces large scale flexural deformation of the surrounding crust, irrespective of whether gravity or surface processes are included (Figure DR7A). This deformation is observed for a wide range of layer thicknesses (Figure DR7B) and fault dips (Figure DR7C). Figure DR8 shows results from a model designed to test the role of in-plane stresses. The model considers a thrust fault with a 1000 m throw that cuts completely through a 30 km thick lithosphere, with different levels of in-plane stress (0, 100 and 1000 MPa). Results show that even for a high in-plane stress of 1000 MPa, the difference between the three flexural profiles is on the order of several 10's of meters, certainly much less than the total fault throw.

FIGURE CAPTIONS FOR SUPPLEMENTARY FIGURES

Figure DR1. Model setups used in the large strain finite element calculations. A constant boundary velocity is imposed at the right hand boundary. Other boundaries are free slip in the boundary-parallel direction, while the upper surface is free to deform and subject to erosion and sedimentation. A light crust overlies a denser Maxwell viscoelastic fluid. In (A) the upper brittle layer includes the entire crust, while in (B) the brittle layer is 20 km thick.

Figure DR2. Time evolution of numerical model of coupled mountain belt - foreland system with inefficient surface processes and a 30 km thick elastic-plastic layer. Magenta coloured region is viscoelastic mantle, green-blue layers are passive markers in the elastic-plastic crust, gray layers near the surface are sediments deposited during the simulation. Parameter values are listed within the text of the Supplementary file.

Figure DR3. Time evolution of numerical model of coupled mountain belt - foreland system with efficient surface processes and a 30 km thick elastic-plastic layer. Magenta coloured region is viscoelastic mantle, green-blue layers are passive markers in the elastic-plastic crust, gray layers near the surface are sediments deposited during the simulation. Parameter values are listed within the text of the Supplementary file.

Figure DR4. Time evolution of numerical model of coupled mountain belt - foreland system with inefficient surface processes and a 20 km thick elastic-plastic layer. Magenta coloured region is viscoelastic mantle, green-blue layers are passive markers in the elastic-plastic crust, uniformly blue coloured region is viscoelastic lower crust, gray layers near the surface are sediments deposited during the simulation. Parameter values are listed within the text of the Supplementary file.

Figure DR5. Time evolution of numerical model of coupled mountain belt - foreland system with efficient surface processes and a 20 km thick elastic-plastic layer. Magenta coloured region is viscoelastic mantle, green-blue layers are passive markers in the elastic-plastic crust, uniformly blue coloured region is viscoelastic lower crust, gray layers near the surface are sediments deposited during the simulation. Parameter values are listed in text of the Supplementary file.

Figure DR6. Numerical models of fully coupled mountain belt - foreland systems developed in the face of inefficient (a) and relatively efficient (b) surface processes, respectively. Calculations performed using the model setup illustrated in Fig. DR1b. Thickness of the elastic-brittle layer is 20 km, compared to 30 km in Figure 1 (main text). Cross sections after 41 Myr of convergence at a rate of 2 mm/yr show sedimentary basins (yellow shade), total rock uplift (dotted line above topography) deformed finite strain markers and base of the crust (blue line). Inset panels illustrate synthetic stratigraphy with time lines plotted every 6.2 Myr. Red lines are flexural profiles calculated with a model of a broken elastic beam loaded with the topography observed in the dynamic model. Parameter values are listed within the text of the Supplementary file.

Figure DR7. Deformation induced by faulting of an elastic layer. Results calculated with a plane strain finite element model showing vertical displacement at the surface induced by slip on a reverse fault cutting an elastic layer that overlies a denser viscoelastic medium. Model output shows final displacements after complete relaxation of gravitational and elastic stresses by viscous flow in the lower layer. **A** Three scenarios involving 10 m of slip on a 30° dipping fault cutting a 30 km thick layer: (1) no erosion and deposition (blue curve), (2) complete rapid erosion of the upthrust block along with complete filling of the basin (green curve) and (3) no gravity. **B** Influence of varying depth of faulting (=thickness of elastic layer) on vertical displacements at surface induced by 10 m of slip on a 30° dipping reverse fault. Surface processes are neglected. **C** Influence of varying fault dip on surface displacements induced by slip on a reverse faulting cutting a 30 km thick elastic layer. Each fault has the same amount of vertical offset on the fault, thus implying a different amount of horizontal slip. Surface processes are neglected.

Figure DR8. Influence of in-plane stress on vertical deflection adjacent to a reverse fault (throw = 1 km) cutting a 30 km thick crust (ρ=2800 kg/m^3) resting on a more dense viscoelastic mantle (ρ=3300 kg/m^3). Model output shows final surface displacements after complete relaxation of gravitational and elastic stresses by viscous flow in the lower layer. The figure shows vertical surface displacements for three different in-plane stresses (0, 100 and 1000 MPa) for a 30° dipping fault (A) and for three different fault dips and a high in-

plane stress of 1000 MPa (B). The results show that the stress-induced vertical deflections (i.e., the difference between the curves) are quite small in comparison to the total fault throw, even when the in-plane stress is relatively high (i.e. 1000 MPa).

REFERENCES

Jaeger, J., Cook, N.G. and Zimmerman, R., 2007, Fundamentals of Rock Mechanics, 4th edition Blackwell Publishing, Oxford, p. 475.

Melosh, H. J., and Raefsky, A., 1981, A simple and efficient method for introducing faults into finite element computations.: Bulletin of the Seismological Society of America, v. 71, p. 1391-14000.

Simpson, G. D. H., 2006, Modelling interactions between fold-thrust belt deformation, foreland flexure and surface mass transport.: Basin Research, v. 18, p. 125-143.

Simpson, G. D. H., and Schlunegger, F., 2003, Topographic evolution and morphology of surfaces evolving in response to coupled fluvial and hillslope sediment transport.: Journal of Geophysical Research, v. 108, p. 2300.

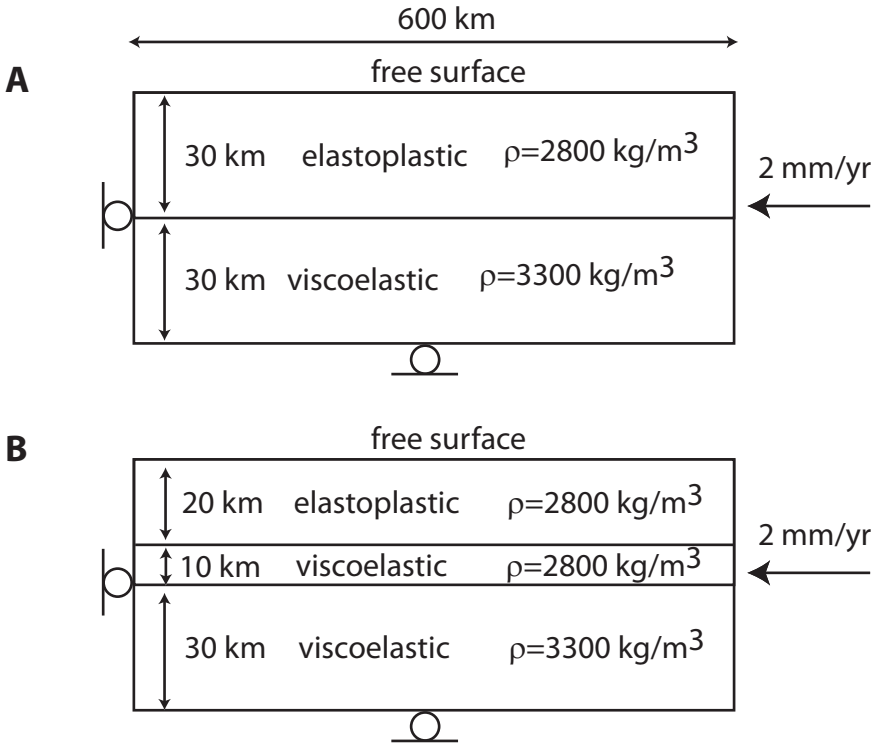
A
600 km
free surface
30 km elastoplastic ρ=2800 kg/m3
2 mm/yr
30 km viscoelastic ρ=3300 kg/m3
B
free surface
20 km elastoplastic ρ=2800 kg/m3
2 mm/yr
10 km viscoelastic ρ=2800 kg/m3
30 km viscoelastic ρ=3300 kg/m3

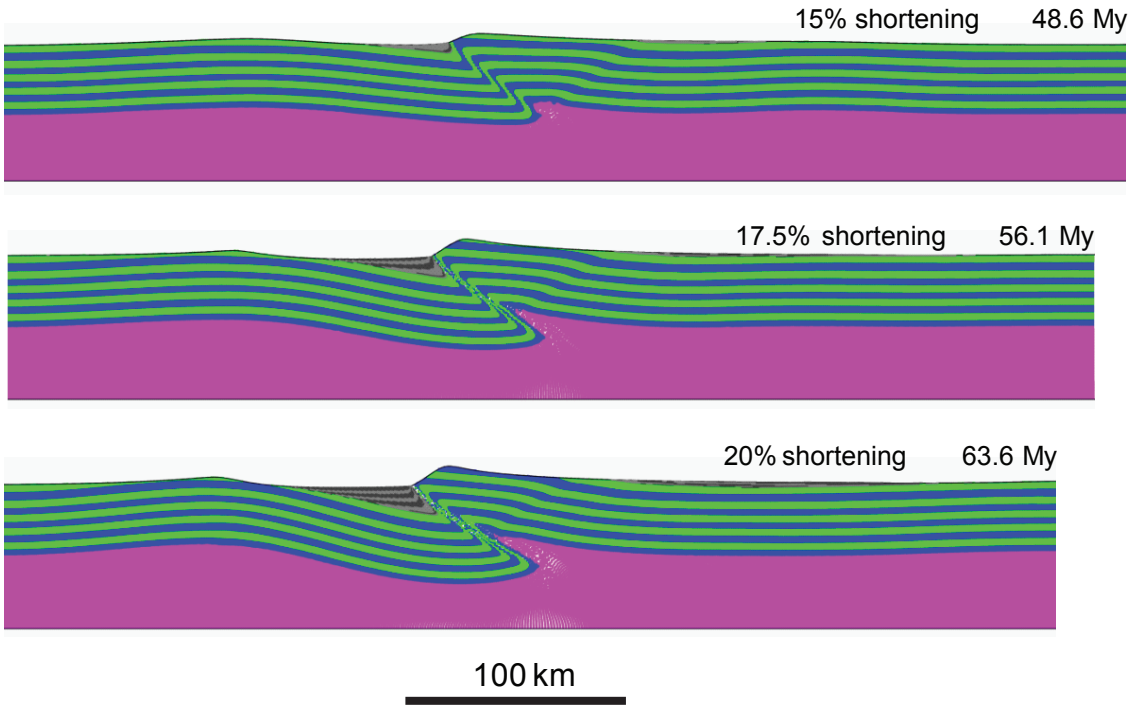
15% shortening
48.6 My
17.5% shortening
56.1 My
20% shortening
63.6 My
100 km

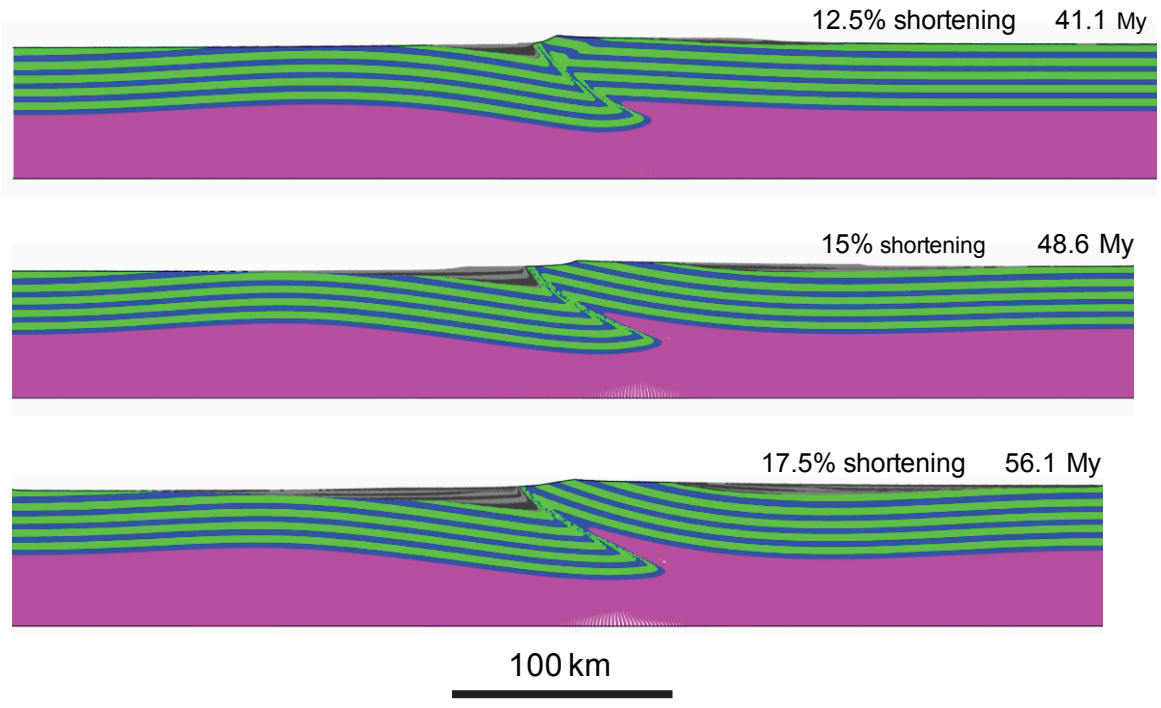
12.5% shortening
41.1 My
15% shortening
48.6 My
17.5% shortening
56.1 My
100 km

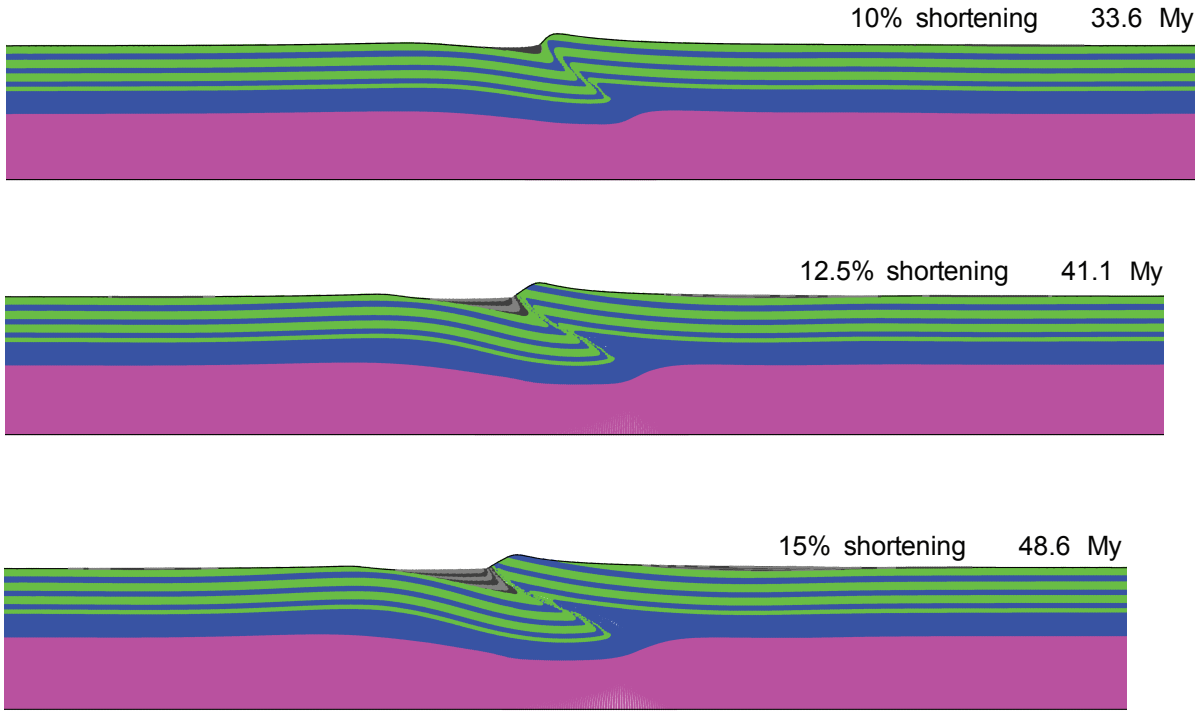
10% shortening 33.6 My
12.5% shortening 41.1 My
15% shortening 48.6 My
100 km

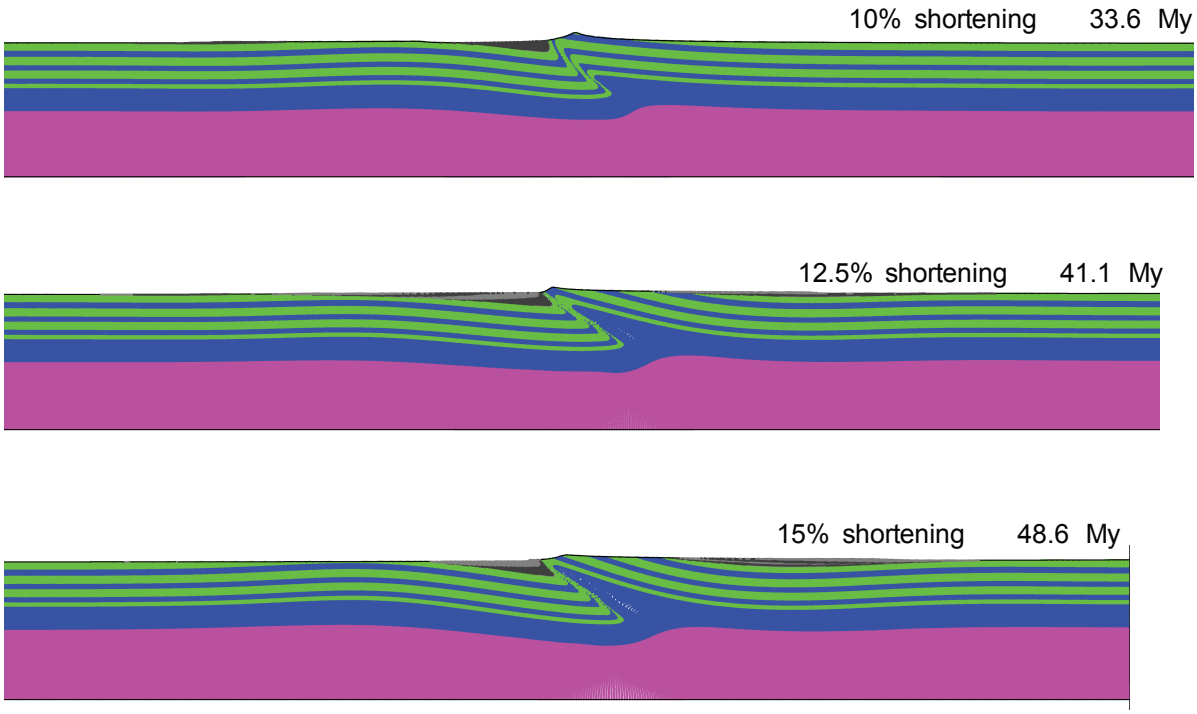
10% shortening 33.6 My
12.5% shortening 41.1 My
15% shortening 48.6 My
100 km

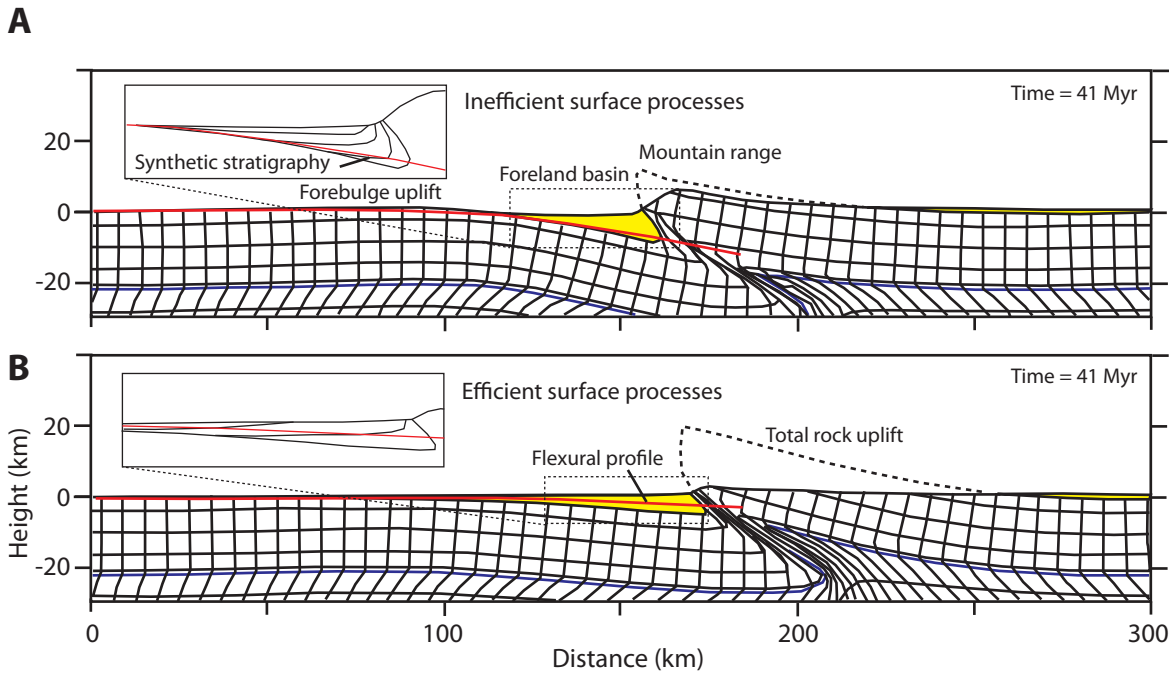
A
Inefficient surface processes
Time = 41 Myr
Synthetic stratigraphy
Forebulge uplift
Foreland basin
Mountain range
20
0
-20
B
Efficient surface processes
Time = 41 Myr
Total rock uplift
Flexural profile
Height (km)
20
0
-20
0
100
200
300
Distance (km)

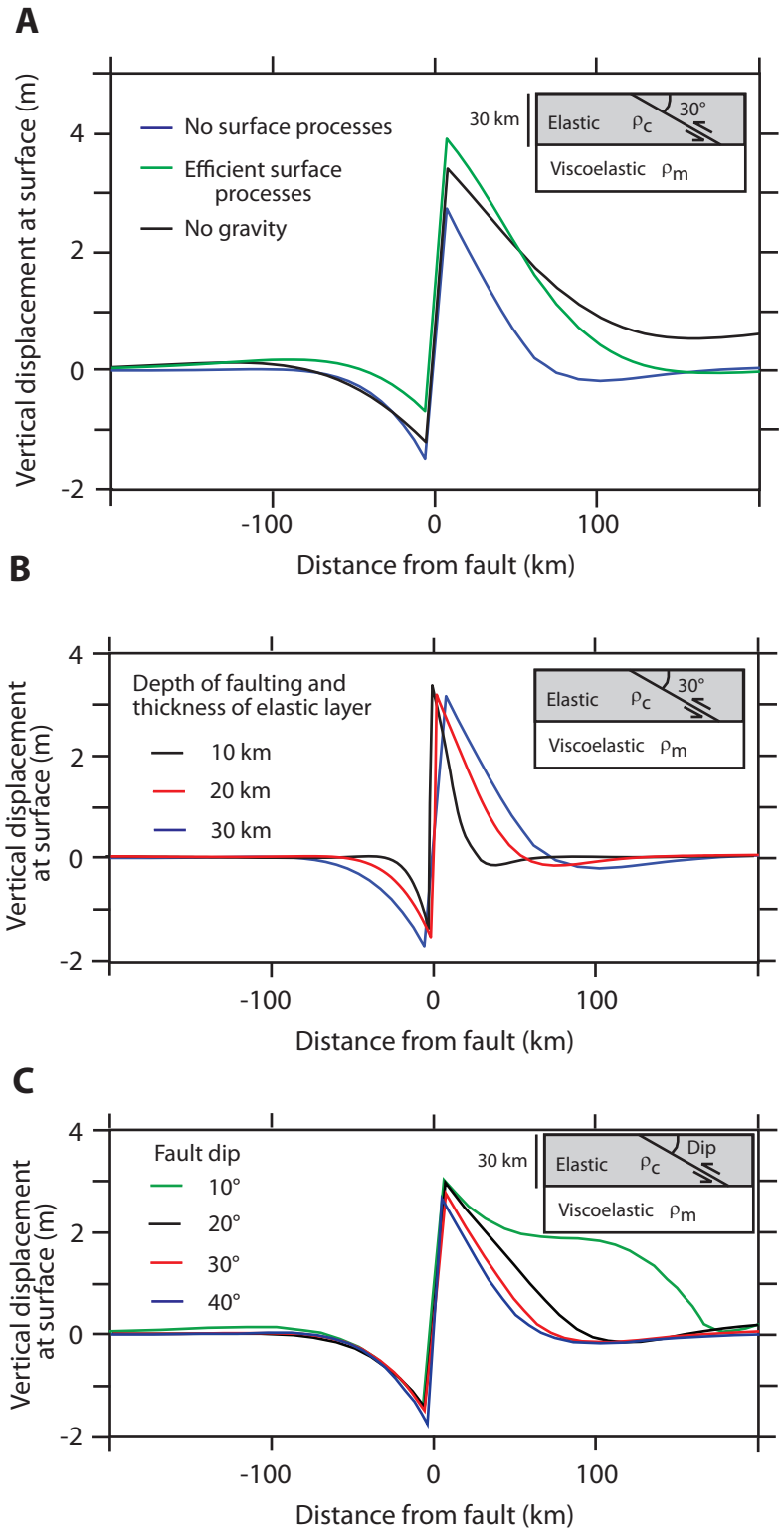
A
Vertical displacement at surface (m)
4
2
0
-2
-100
0
100
Distance from fault (km)
No surface processes
Efficient surface processes
No gravity
30 km
Elastic
ρ_c
30°
Viscoelastic
ρ_m
B
Vertical displacement at surface (m)
Depth of faulting and thickness of elastic layer
10 km
20 km
30 km
Elastic
ρ_c
30°
Viscoelastic
ρ_m
Distance from fault (km)
C
Vertical displacement at surface (m)
Fault dip
10°
20°
30°
40°
30 km
Elastic
ρ_c
Dip
Viscoelastic
ρ_m
Distance from fault (km)

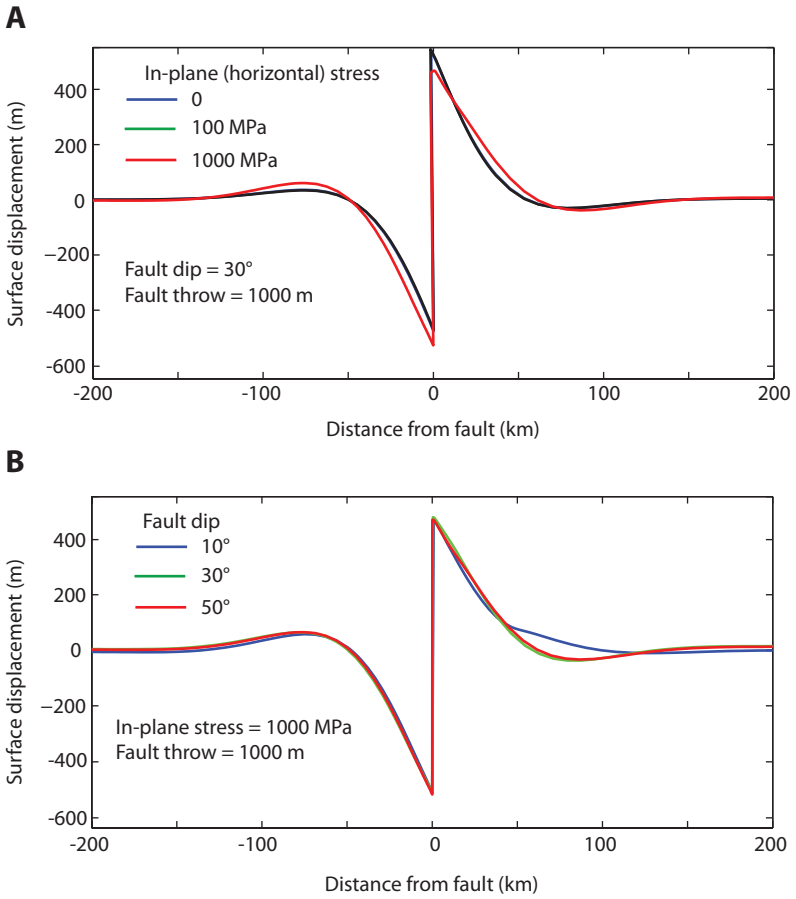
A
In-plane (horizontal) stress
0
100 MPa
1000 MPa
Fault dip = 30°
Fault throw = 1000 m
Surface displacement (m)
400
200
0
−200
-400
-600
-200
-100
0
100
200
Distance from fault (km)
B
Fault dip
10°
30°
50°
In-plane stress = 1000 MPa
Fault throw = 1000 m
Surface displacement (m)
400
200
0
−200
-400
-600
-200
-100
0
100
200
Distance from fault (km)